Int. J. Electrochem. Sci., 16 **(2021)** Article Number: 211241, doi: 10.20964/2021.12.43

International Journal of
ELECTROCHEMICAL
SCIENCE
www.electrochemsci.org

Electrochemical Photocatalytic Degradation of Rhodamine B Dye by Sm^{3+} doped Titanium Dioxide (Sm-TiO_2) in Natural Sunlight Exposure

Zaid H. Mahmoud[1,2], *Reem Adham AL-Bayati*[1] *and Anees A. Khadom*[3,*]

[1] Department of Chemistry, College of Science, Al-Mustansiriyah University, Baghdad, Iraq.
[2] Department of Chemistry, College of Science – University of Diyala – Baquba City 32001, Diyala governorate, Iraq
[3] Department of Chemical Engineering, College of Engineering – University of Diyala – Baquba City 32001, Diyala governorate, Iraq
[*]E-mail: Zaidhameed_91@yahoo.com

Received: 5 September 2021 / *Accepted:* 18 October 2021 / *Published:* 10 November 2021

Nanoparticles Sm-TiO_2 is successfully synthesize by photolysis method for degrading Rhodamine B (RhB) dye under direct sunlight. The prepared nanoparticles were characterized by X-photoelectron spectrum (XPS), X-ray diffraction (XRD), Raman spectrum, field emission scanning electron microscope-energy dispersive x-ray (FESEM-EDX) and UV-Visible spectrum (UV-Vis). The XPS spectrum revealed that 1% Sm-TiO_2 was successfully doped. The results from XRD and Raman showed the formation of anatase phase for prepared and doped TiO_2. According to the Debye Scherrer equation, particle size decreased as Sm^{3+} concentration increased, reaching 4.56 nm at 5% Sm-TiO_2. For the synthesized material, FE-SEM revealed a spherical agglomeration. The UV-Vis spectrum revealed that the energy gap decreased as the concentration of dopant (Sm^{3+}) increased. Cyclic voltammetry (CV), electrochemical impedance spectroscopy (EIS), and chronopotentiometry (CP) were used to examine the electrochemical characteristics of pure and Sm:TiO_2 under dark and light conditions. The results show that the catalyst behaves as a pseudocapacitor when the Sm^{3+} ratio rises, as does the conductivity.

Keywords: electrochemical; rare earth, photolysis, cyclic voltammetry; impedance; chronopotentiometry.

1. INTRODUCTION

The hazardous and toxicity of organic and dye materials, until in low concentration, has a harmful effect on ecological systems [1-3]. It discharges a significant amount of contaminants into the water, resulting in nondurable water. Dyes inhibit photosynthesis by preventing the passage of light, resulting in low dissolved oxygen levels in the water [4-6]. Fenton, activated carbon adsorption, and

other techniques were utilized to remove and reduce the dyes. Despite their efficacy, these approaches have considerable disadvantages. The Fenton approach, for example, requires a large volume of reagent, and activated carbon removes the color with some contamination [7, 8]. Photon-based oxidation technique is one way to degrade the dye without using reagents or producing hazardous by-products. Because of the eco-friendly technology, free energy, and renewable nature of this method, it has received a lot of attention. Additionally, the use of sunlight as a source for photo deterioration makes it more commercially viable [9-11]. TiO_2 has exhibited good and considerable potential in removing and reducing dye contaminants and bacteria from sewage, owing to its interesting properties in terms of photoactivity, stability, availability, and low-cost. It is the most active photocatalyst because of a wide energy gap (3.2 eV) and adsorb nearly 5% from incident sunlight photon. However, this is insufficient to prevent dye degradation. Doping with transition ions can be used to develop a dynamic way of shifting anatase band gap adsorption to the visible area. Transition metal ions with an d-electron unfilled orbital have the authority to transfer electrons from the 3d level of the dopant ions to the band conduction of TiO_2 to accommodate more electrons and trap photogenerated electrons or holes, reducing their recombination and shifting the optical response of TiO_2 toward higher wavelengths. The goal of this research is to improve the portability of TiO_2 as a photocatalyst for adsorbing incident sunlight photons by doping it with various Sm^{3+} ratios. The utilize of lanthanide metals in doping helps to reduce the rate of recombination process [12]. Xin and Yuan [13] reported the activity of Nd-TiO_2 as a photocatalyst for degradation of phenol under sunlight. Li [14] examined the activity of Ce-TiO_2 as photocatalyst under UV and visible light. Many methods were reported for synthesis of lanthanide doping TiO_2 such as precipitation, sol-gel and hydrothermal methods [15-17].

This study represented a promising photolysis method with low cost and more efficiency for synthesis of Sm-TiO_2 powder. The product was characterized by the XPS, XRD, Raman spectrum, FE-SEM-EDS and Uv-Vis spectrum. The activity of catalyst was studied and investigated on degradation of RhB dye in suspension of 1,3 and 5% Sm-TiO_2 under sunlight and the results were compared to Sm^{3+} free TiO_2.

2. MATERIALS AND METHODS

Samarium nitrate hexahydrate, titanium (IV) isopropoxide and ethylene glycol were supplied from sigma aldrich chemicals company. Hydrochloric acid, sodium hydroxide and Rhodamine B were of the analytical grade. The molecular weight of dye is 479g/mol and lamda max = 556nm.

2.1 Preparation of Sm-TiO_2

(1,3, and 5%) weigt ratio Sm doped TiO_2 were prepared through photolysis method by mixing equivalent quantities of $Sm(NO_3)_3.6H_2O$ and $Ti[OCH(CH_3)_2]_4$. Individually, each 200ml mixture was transferred to the irradiation system of 125W as shown in Fig. 1. The full procedure of irradiation system was reported by Zaid et al. [18]. The mixture was irradiated for one hour under a surfactant and capping agent of dropped 5ml ethylene glycol. The white powder was separated and washed with 20ml

of ethanol, acetone, and distilled water numerous times. It was then dried for 4 hours at 70 °C before being calcined for 4 hours at 400 °C.

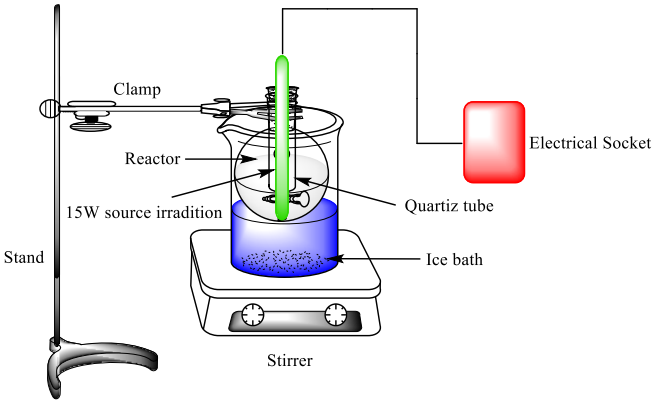

Figure 1. irradiation system with 125W power

2.2. Photocatalytic activity of Sm-TiO_2

The degradation of RhB dye under sunlight was used to investigate the photoactivity of Sm-TiO_2 catalyst. Three reactors were treated with a 30 ppm natural RhB solution before being irradiated. One without catalyst and two with 0.01gm catalyst were maintained in the dark and agitated for 30 minutes until adsorption – desorption equilibrium was reached. Experiments with various circumstances were conducted for 2 hours between 10 and 12 a.m. in October/2020, with an average intensity of 1200 $W.cm^{-2}$ sunlight.

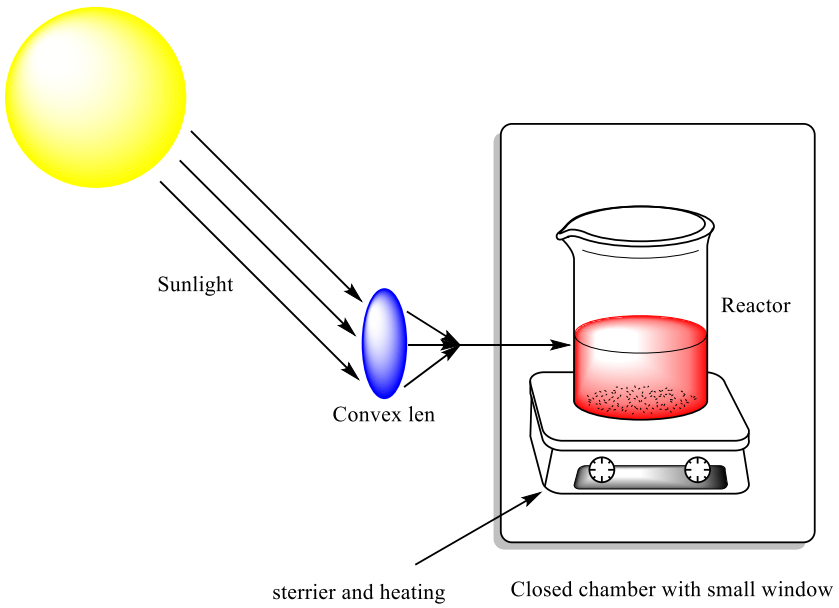

Figure 2. Diagram of Photodegradation process

Through the use of a convex lens, the intensity of sunlight was focused on the reaction system. Fig. 2 shows a systematic diagram of degradation. Except for the activation energy estimates, all of the parameters were measured at room temperature. At a specific time, aliquots were taken from the reactor and centrifuged to remove the catalyst. The UV-Vis spectrum was used to record the adsorption of transparent dye solution.

2.3 Characterization and measurements

The structure of synthesized (Sm-TiO_2) were investigated and recorded by Shimadzu x-ray diffraction using CuKα radiation and λ =1.5406 A^o with an accelerating voltage equal 30KV as well as, the diffractogram was displayed with the range of 2θ = 10^o-80^o. X-ray photoelectron microscopy (XPS) spectra was showed using spectrometer of a Kratos AXIS 165 with aluminum (Al) mono K-alpha X-ray to evaluate of chemical state. The morphology of synthesized materials were performed using field emission scanning electron microscope (ZEISS) and transmission electron microscope (JEOL JEM 2100). The spectra of Raman was done by microscope of laser Raman (Raman 11i) with wavelength of 525nm. The spectral properties was evaluated using UV-VIS spectrophotometer (Jasco-V-650). The electrochemical properties were investigated using electrochemical impedance spectroscopy (EIS) utilizing Solarton gain phase analyzer.

3. RESULTS AND DISCUSSION

3.1. Characterizations of Sm-TiO_2 structure

3.1.1 XPS measurements

The XPS spectrum was carried out to investigate the composition, type and nature of species found in the structure of 1%Sm-TiO_2 and pure TiO_2 nanoparticles (Fig. 3A – D). In Fig. 3A, the spectrum shows the producing of Ti, Sm, O and a trace of C. These traces in the structure can be considered as a contamination that may be adsorbed during the synthesis of nanoparticles. Due to the change in the electron environment of Ti^{4+} after doping with 1% Sm and formation of Sm-O-Ti bonds, the two peaks attributed to Ti $2p_{3/2}$ and Ti $2p_{1/2}$ situated at 458.7 and 464.3 eV as seen in Fig. 3C migrated towards high binding energy compared to pure TiO_2. This result was also reported in the literature [19]. In comparison to pure anatase, the shift in binding energy of O 1s of Sm:TiO_2 was identical to that seen for the Ti 2p state (Fig. 3B). Due to the presence of Sm in Anatase's structure, two binding energies centered at 1083.1 and 1110 eV were attributed to Sm $3d_{5/2}$ and $3d_{3/2}$ levels (Fig. 3D). Sm^{3+} is included in the structure of TiO_2 according to all XPS studies [19].

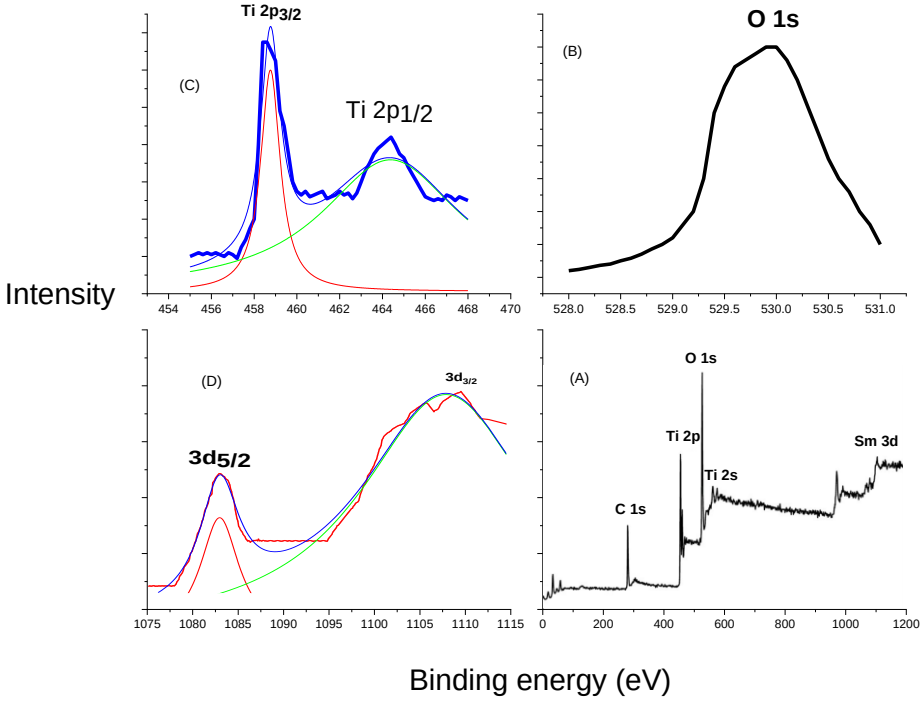

Figure 3. XPS spectrum of 1%Sm-TiO2, (A) survey spectrum, (B) O 1s, (C) Ti 2p and (D) Sm 3d

3.1.2. XRD measurements

The X-ray diffraction of TiO_2, Sm_2O_3, and 1, 3, 5% Sm:TiO_2 that synthesized by photolysis method and calcined at 400°C were shown in Fig. 4.

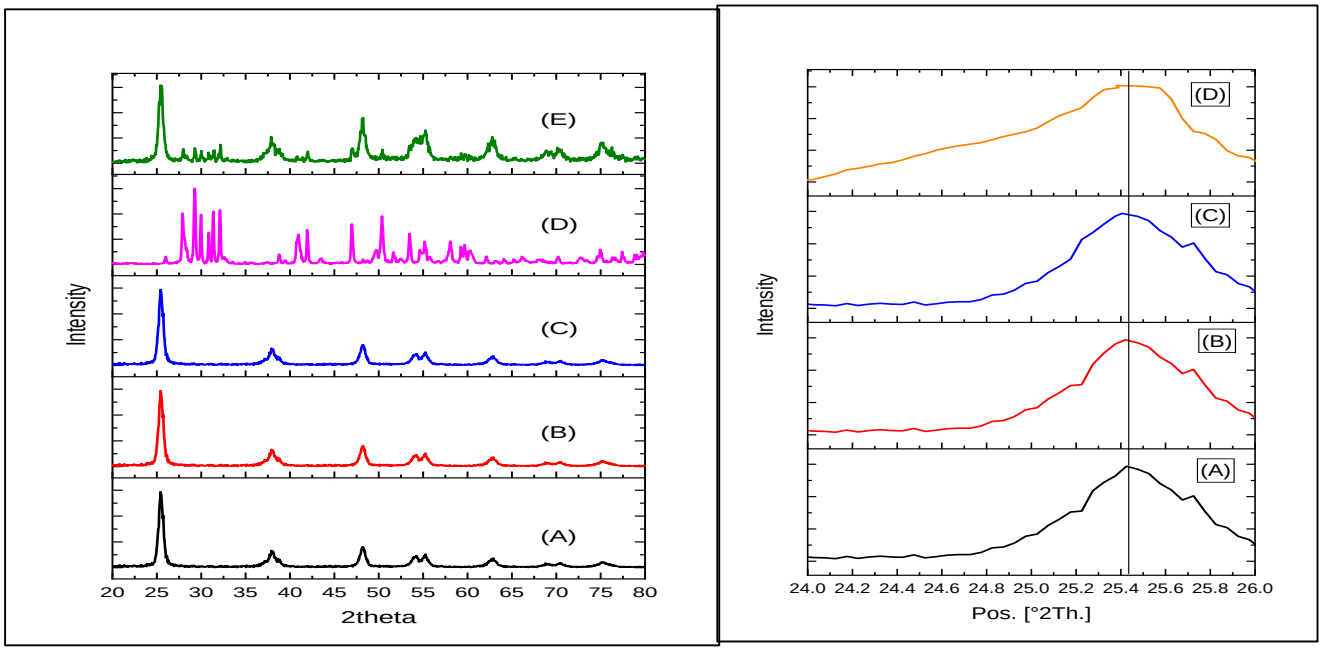

Figure 4. XRD of (A) TiO_2, (B) 1%Sm-TiO_2, (C) 3%Sm-TiO_2, (D) Sm_2O_3 and (E) 5%Sm-TiO_2

The values of 2theta and Miller indices were 25.35º (101), 37.78º (004), 48.07 º (200), 53.92 º (105), 55.11º (211), and 62.72º (204), respectively. It attributed to anatase phase of TiO_2 according to JCPDS no. [04-0477]. All Sm^{3+} dopant concentrations in the TiO_2 matrix exhibited anatase phase, indicating that all dopants, regardless of concentration, stabilized TiO_2 anatase phase. Using the Scherrer equation, the crystallite size of pure anatase and varied ratios of Sm^{3+} dopant with anatase were determined (Eq. 1).

$$D = \frac{0.9\,\lambda}{\beta \cos\theta} \qquad 1$$

where 0.9 is the shape factor, λ is the wavelength of the X-ray source, and β is the full width at half maximum of the peak concerned. The results showed that in comparison to pure TiO_2, the diffraction peaks become broader in width as the doping ratio of Sm^{3+} increases, shifting to low locations as illustrated in Fig. 4.

This indicate that segregation of Sm^{3+} at grain boundary of TiO_2 anatase phase decreases the size of crystal [17], but the shift in location causes an increase in d-spacing because high ionic radii Sm^{3+} penetrate the matrix of anatase and are replaced by Ti^{4+} [20]. The results are shown in table 1.

Table 1. Size of particles of TiO_2 and %Sm-TiO_2

Photocatalyst	**2θ of crystal plane (101) of TiO_2**	**Lattice parameter (A)**	**FWHM**	**Crystallite size (nm)**
TiO_2	25.46	a=b=3.78 c=9.5023	0.67036	12.92
1%Sm:TiO_2	25.38	a=b=3.78 c=9.5123	*0.96822*	*8.27*
3%Sm:TiO_2	25.29	a=b=3.78 c=9.5211	*1.49543*	*5.33*
5%Sm:TiO_2	25.21	a=b=3.78 c=9.5307	*1.74390*	*4.56*

The XRD of 1% and 3% Sm-TiO_2 shown in Fig. 4B and C shows no characteristics peaks corresponding to Sm^{3+}, which suggest that the Sm^{3+} incorporated in the crystalline of anatase or may be back to dispersed with values lower than the critical value of dispersion capacity, preventing the formation of a crystalline with separate phase. To analyze the lattice characteristics of prepared samples, the typical peaks (101), (200), and (004) of TiO_2 anatase phase were chosen. The results show (table .1) slight elongation of c axis while a and b remained almost constant. The marginal changes in c axis indicate that the Sm^{3+} dopant occupied bcc and fcc positions in the structure of anatase [21].

The size of the crystallite has a definitive effect on the deep/shallow trap of charge carriers photogenerated by the catalyst samples. There are two routes for carrier charge recombination in pure TiO_2: (i) surface recombination and (ii) volume recombination. The volume recombination process is dominating at large particle sizes, and the average length of charge carrier diffusion paths to the

surface becomes longer, causing deep entrapment and decreased activity. The crystallite size of prepared Sm:TiO_2 are 8.27, 5.33 and 4.56nm for the dopant concentration of 0, 0.01, 0.03 and 0.05 respectively. The reduction in the size of particles increases the surface area and variable active site resulting in increased photonic efficiency. Additionally, the reduction in crystallite size reduces the length of diffusion path for carrier of charges from the site that which photogenerated to reaction site. This reduction lead to reduce in rate of recombination which cause increasing the efficiency of photocatalyst as it observed in 5%Sm-TiO_2 [21].

3.1.3 Raman spectrum measurements

Raman spectrum was used to determine the phase transition and the crystal structure of compound [22]. Fig. 5 shows the Raman spectrum of pure and 3%Sm-TiO_2.

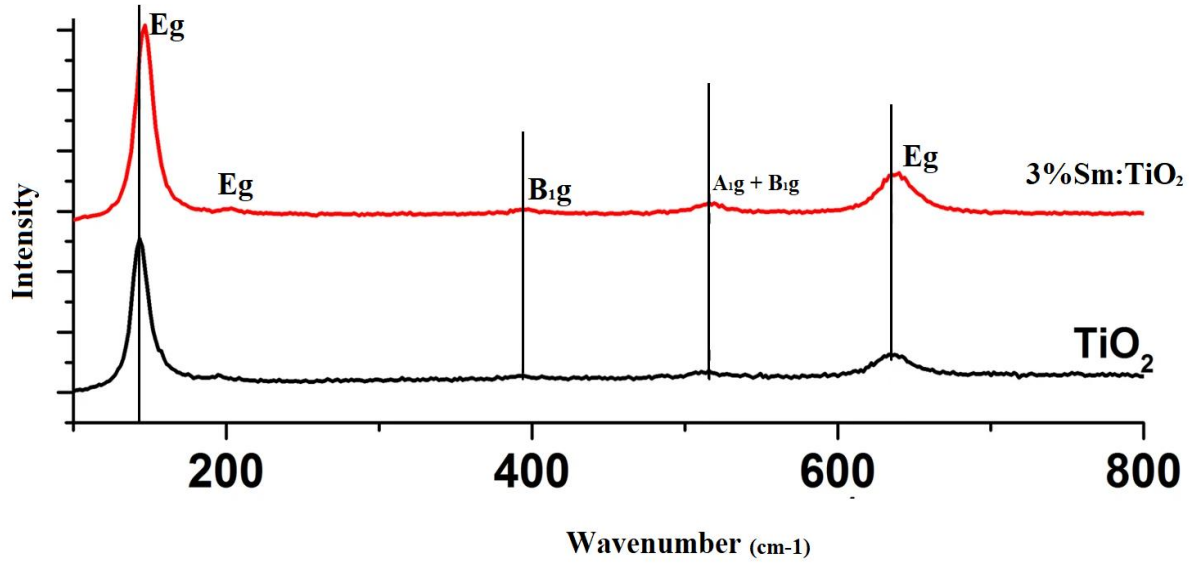

Figure 5. Raman spectrum of 3%Sm-TiO_2.

The anatase phase was visible due to the position of the peaks. Six peaks are ascribed to Eg at 144, 195, and 638, while 398 and 518 are allocated to B_1g, and 513 is assigned to A_1g [23]. Similar results for the Raman spectra of pure anatase have been reported in the literature [24]. After doping Sm, a shift in spectrum was noticed, indicating that Sm doping has no effect on the crystal structure of TiO_2. Furthermore, the intensity of peaks decreased after doped by Sm^{3+} because the disorder into the lattices of anatase.

3.1.4. FESEM-EDX measurements

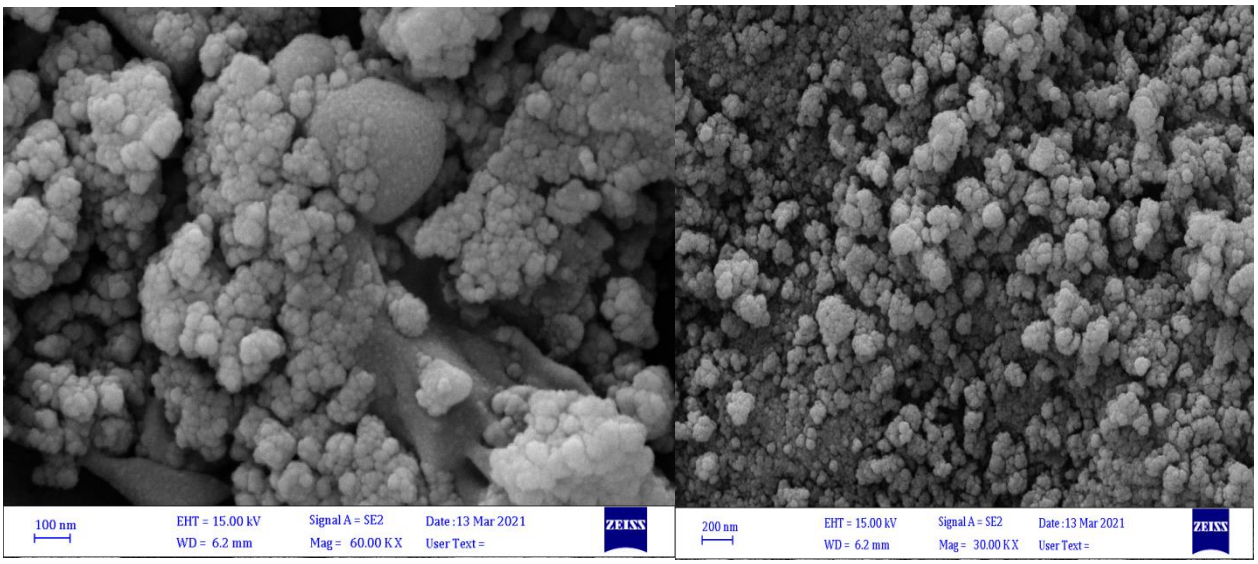

Figure 6. FESEM of 5%Sm:TiO_2.

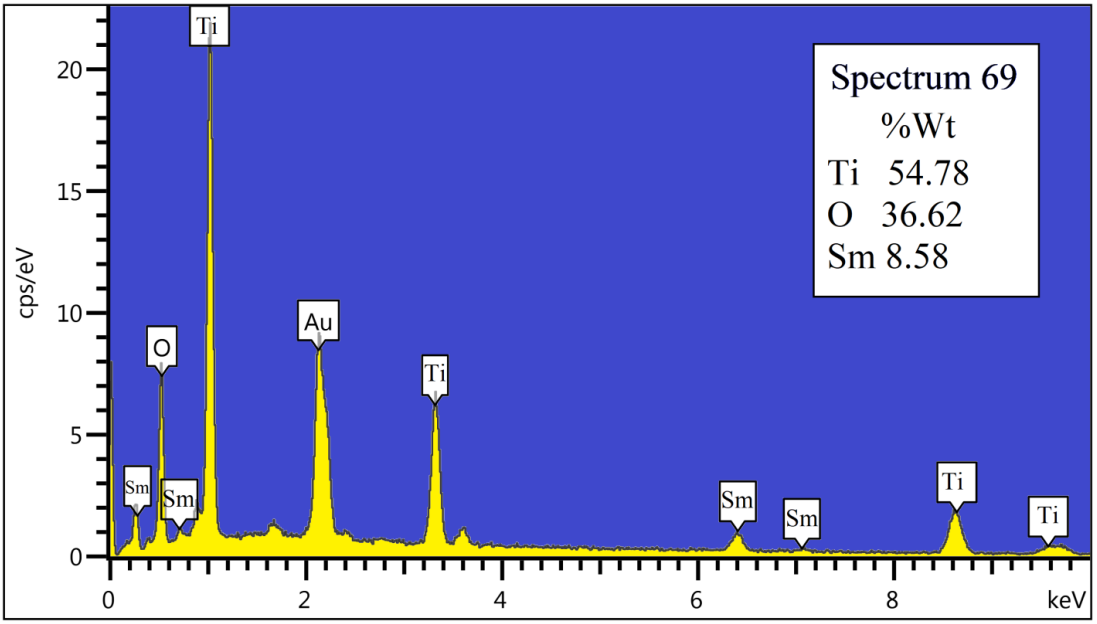

Figure 7. EDX spectrum of 5%Sm:TiO_2

FESEM-EDX was used to analyze the shape and ratios of each element in the structure of 5% Sm-TiO_2 as shown in Fig.6 and 7. It was discovered that the adopted synthesis technique resulted in the agglomeration of spherical particles, indicating a low level of morphological control. The particle sizes measured by FESEM were consistent with those obtained by XRD. EDX analysis was used to analyze the ratio of components present in the structure of the produced compound. EDX analysis was used to analyze the ratio of components present in the structure of the produced compound. The great purity of Sm:TiO_2 nanoparticles is seen in Fig. 7. The presence of Au is related to the base utilized in

Sm-TiO_2 precipitation. The computed percentages of components accord well with the practical calculation of doping 5% of Sm_2O_3 with TiO_2.

3.1.5. UV-Visible spectrum and total organic carbon (TOC)

The adsorption mode of UV-Vis measurements was conducted to investigated the electronic structure and effect of doping Sm on the band gap of TiO_2. The decolorization profile of RhB dye using %5Sm-TiO_2 is present in Fig. 8a. In Fig. 8b, however, the percentage degradation of dye over pure TiO_2 and 5% Sm:TiO_2 is shown, with the Sm-TiO_2 catalyst showing a greater deterioration. In the first 20 minutes of sun exposure, 5%Sm-TiO_2 demonstrated a 43% decolorization compared to 8% for pure TiO_2. After 120 minutes in the sun, the percentage of dye degradation reached 89%. In Fig. 8c, the constant of rate "k" for dye degradation in the presence of pure TiO_2 and Sm-TiO_2 is graphically investigated using the Langmuir-Hinshelwood kinetic. k= 0.02094min-1 was found for 5% Sm-TiO_2, compared to k= 0.009214min-1 for pure TiO_2. When compared to pure TiO_2, the high degradation or decolorization of doped TiO_2 indicates that the presence of Sm in the matrix of TiO_2 results in a high efficiency in the transmission of photo-excited electrons.

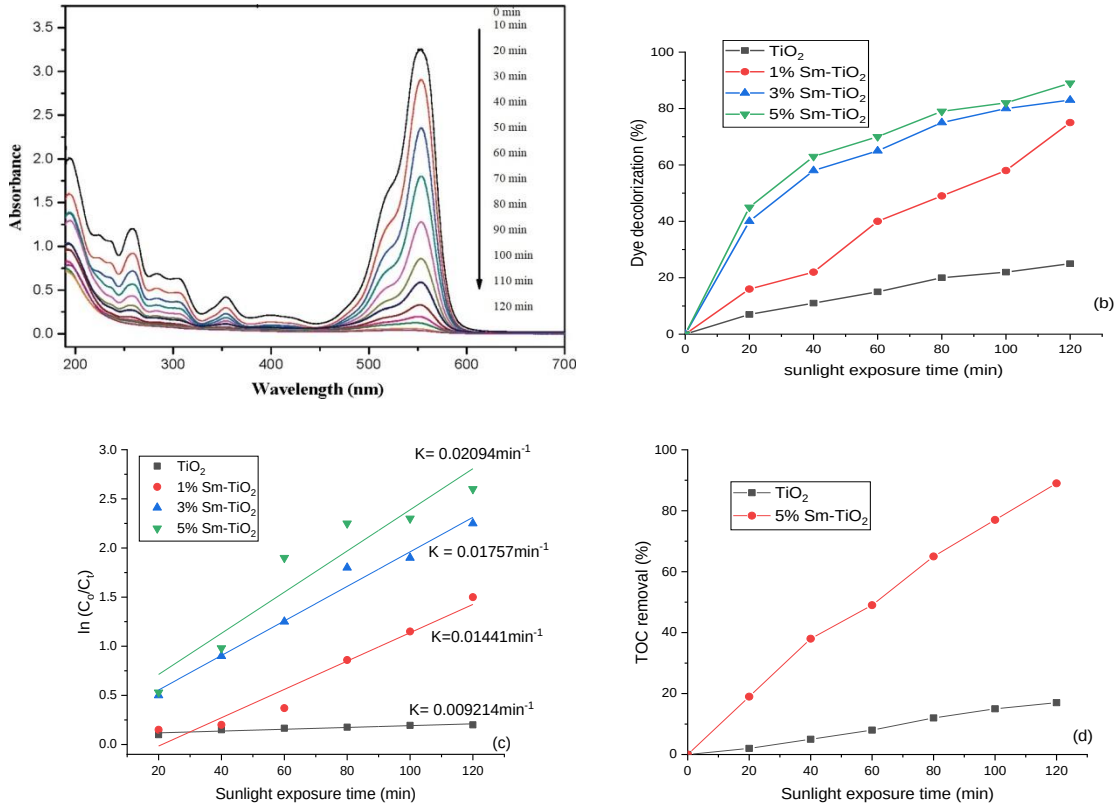

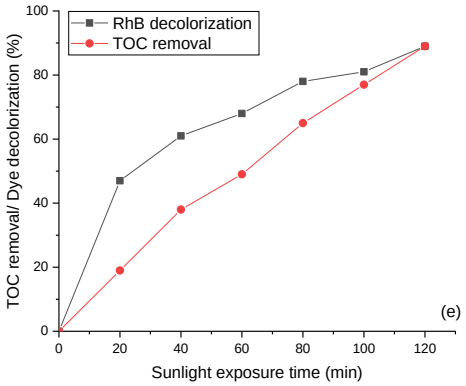

Figure 9. a the UV-Vis spectrum decolorization of RhB at different times over 5%Sm-TiO_2, **b** comparison of decolorization RhB over pure and Sm-TiO_2, **c** the graphic investigation of decolorization rate, **d** TOC removal of RhB dye over pure and Sm doped TiO_2 and, **e** comparison of decolorization and mineralization of RhB dye over 5%Sm-TiO_2

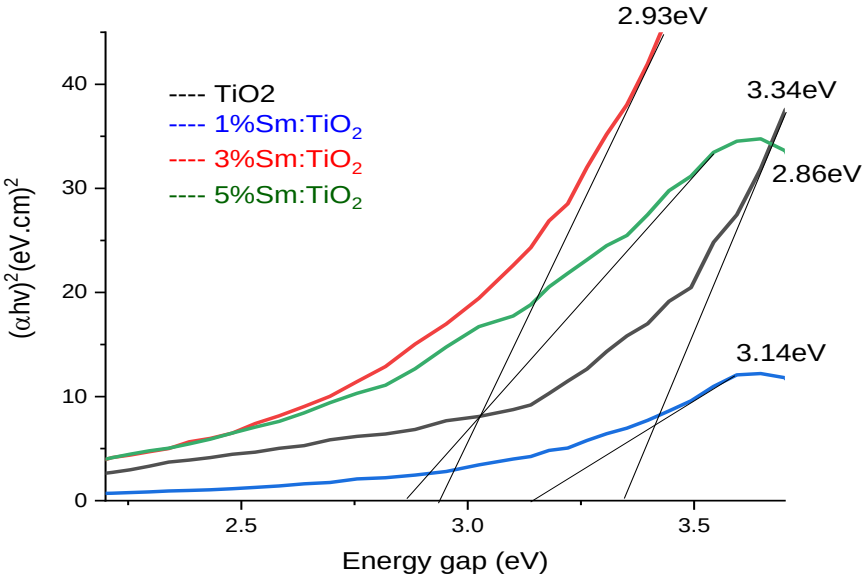

Figure 9. Energy gap of (A) TiO_2, (B) 1%Sm-TiO_2, (C) 3%Sm-TiO_2, and (D) 5%Sm-TiO_2.

The defeat of pure TiO_2 in decolorization of RhB dye depicts loss of charge carriers in recombination process with suitable potential foe edge of conduction band of anatast TiO_2 (-4.03V) [25] for reduction of oxygen to super anion. As reported [26], the dyes lose their color and band of adsorption with loss conjunction. Any change in the structure of dyes, such as a reaction or the introduction of an oxidizing species into a photocatalytic system, results in a decrease in the strength of the absorption band at a specific wavelength, which is commonly referred to as mineralization or degradation. According to some studies [27], this process is nothing more than decolorization. As a result, rather than degradation or mineralization, the initial reaction between the oxidative species (oxygen super anion or hydroxyl free radical) and the dye molecule produces decolorization and a

range of intermediates. TOC investigates the parameter that can distinguish between decolorization and mineralization. Fig. 8d shows the TOC removal (percentage) as a function of pure TiO_2 and 5 % Sm-TiO_2. The results show that 5% Sm-TiO_2 has 10 times the mineralization of pure TiO_2. The recognizing of a reduction in RhB dye absorption by UV-Vis spectroscopy is not the genuine signal of RhB dye degradation, as shown in Fig. 8e, which illustrates the comparison of mineralization and decolorization for 5%Sm-TiO_2. In comparison to 43% decolorization of RhB in the first 20min of sunlight periphrasis, only 18% of organic carbon was removed in the same period. The difference between uv-vis and TOC measurements indicates that oxidative species (oxygen super anion or hydroxyl free radical) initially react with RhB dye molecules to convert it into intermediate product, which causing fragmentation of it with significant disadvantages to the structure of conjugated that results in decolorization of RhB dye. The pace of removing organic carbon increases as the concentration of RhB dye decreases, indicating the involvement of more oxidizing radicals in the removal of TOC that were previously involved in decolorization. As previously stated, the anatase TiO_2 has a favorable (-4.03V) for oxygen reduction, implying that the production of (O_2•−) is unavoidable. The removal of TOC and rapid decolorization of RhB suggested the active role of (O_2•−) in process of oxidation compared to other species of oxidation such as hydroxyl free radical OH• [28]. The energy gap of synthesized nanoparticles was examined by Taucs relationship (Eq. 2).

$$(\alpha hv)^2 = A(hv - E_g) \quad 2$$

E_g represents the optical band gap, v represents the frequency of incident photons, h is the Planck's constant, and A is a constant called the band tailing parameter. The plot of $(\alpha hv)^2$ versus hν for TiO_2 and doping different ratio of Sm with direct band gap and n=2 were shown in Fig. 9. The direct energy gap in oxide nanoparticles is caused by charge transfers between the 2p of O^{-2} and the vacant 3d orbital of Ti^{4+} in the anatase phase of TiO_2. The electron transitions directly from the valence band (VB) to the conduction band (CB) in pure anatase. The electrons do not direct transition to the conduction band when Sm doping is used because oxygen vacancies and vacant Sm s,d, and f capture the electrons. As a result, the reduced band gap is caused by the sub-band and oxygen defect. With the addition of Sm^{3+}, the band gap of TiO_2 was lowered from 3.29 to 2.77 eV. This decrease might be attributed to a structural defect that grew with increasing Sm concentration, as well as a reduction in particle hybridization between Sm t_2g and O^{-2} 2p states to an empty t_{2g}^* 3d orbital of Ti^{4+}. It could also be attributed to a reduction in in-plane strain [29]. Depending on the obtained results, the sequence of energy gap for fabricated oxides was 5%Sm-TiO_2> 3%Sm-TiO_2> 1% Sm-TiO_2> TiO_2. It was 2.86, 2.93, 3.14, and 3.34 eV, respectively.

3.2 Electrochemical characterization

The electrochemical studies of pure and Sm doped TiO_2 powders was investigated by cyclic voltammetry (CV) and double step chronopotentiometry (CP). Fig. 10a illustrates the comparison curves of CV for pure and Sm doped TiO_2 electrodes recorded at 50mV/s with range +0.6 to -0.1V and 1mM electrolyte of ferricyanide under dark condition. The behavior of pseudo capacitive of pure and Sm:TiO_2 electrodes was assigned to the quasi-reversible forms obtained from CV curves. The electron

transfer pathway for the ferric/ferrous couple was linked to the pair of redox peaks [30] The successful immobilization of photocatalyst on the electrode surface was also demonstrated by the reduction in current density. The major role of Sm^{3+} ions on the surface of anatase TiO_2 as a redox broker seems to be the defective electrical double layer capacitive (DLC) attitude. Under lighting, the 5%Sm-TiO_2 electrode has a greater density peak of current than anatase TiO_2 and other doped electrodes, as well as higher charge transfer ability (Fig. 10b). According to XRD studies [31], the increased conductivity of Sm:TiO_2 photocatalyst was attributed to the synthesis of surface Sm_2O_3.

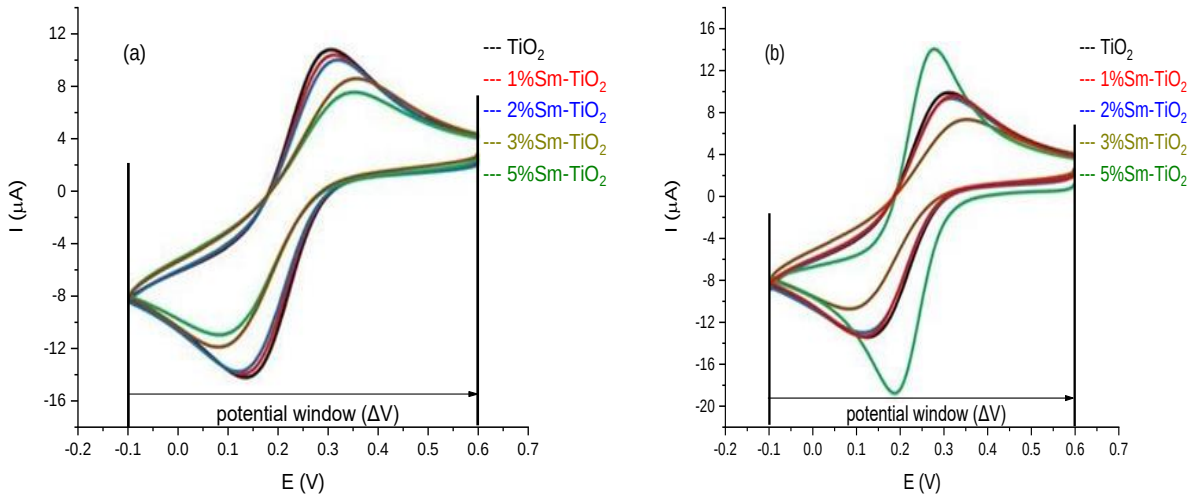

Figure 10. Cyclic voltammetry of pure and Sm:TiO_2 (a) dark and (b) illumination condition

Table 2. The parameter got from Nyquist equation for pure and Sm-TiO_2

Dark				
photocatalyst	R_{ct} (ohm)	R_s (Ohm)	W_z (Ohm/$s^{1/2}$)	C_{dl} (□F)
TiO_2	90.43	22.12	2200	1.06
1%Sm:TiO_2	99.21	22.98	2361	1.53
2%Sm:TiO_2	116.42	21.31	2470	1.24
3%Sm:TiO_2	210.96	24.10	2800	1.03
5%Sm:TiO_2	203.41	22.03	3166	1.22
Under illumination				
photocatalyst	Rct (ohm)	Rs (Ohm)	Wz (Ohm/$s^{1/2}$)	Cdl (□F)
TiO_2	106.21	18.31	2190	1.07
1%Sm:TiO_2	115.78	19.32	2622	1.51
2%Sm:TiO_2	130.52	19.03	2675	1.21
3%Sm:TiO_2	248.42	20.68	3120	0.98
5%Sm:TiO_2	65.27	19.08	3645	0.83

The EIS spectra of pure and Sm^{3+} doped TiO_2 photocatalyst electrodes in dark and light are represent in Fig. 11 a, b. The EIS Nyquist advantage plots for determining electron hole pair separation efficiency and charge resistance are confirmed [32,33]. In Fig. 11a, compared to pure TiO_2, the

presence of large semicircular portions in the EIS Nyquist plot indicated that Sm-TiO_2 has a higher resistance to charge transfer and lower conductivity, whereas the lower resistance to charge transfer for 5% Sm-TiO_2 indicates that it has a higher electrical conductivity (Table. 2).

As shown in Fig. 11b, the addition of a reduction in charge transfer resistance was attributed to the improved conductivity of the 5% Sm:TiO_2 electrode surface under illumination conditions. The results showed that EIS and CV have a good agreement.

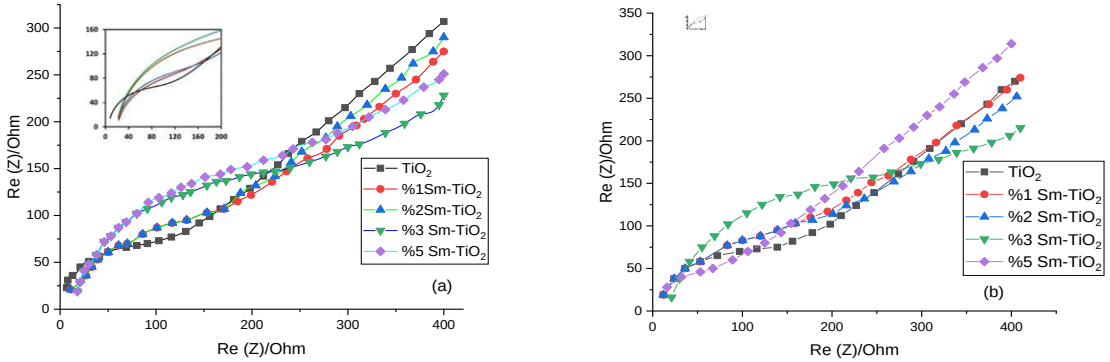

Figure 11. EIS spectrum of pure and Sm-TiO_2 (a) dark, (b) illumination condition

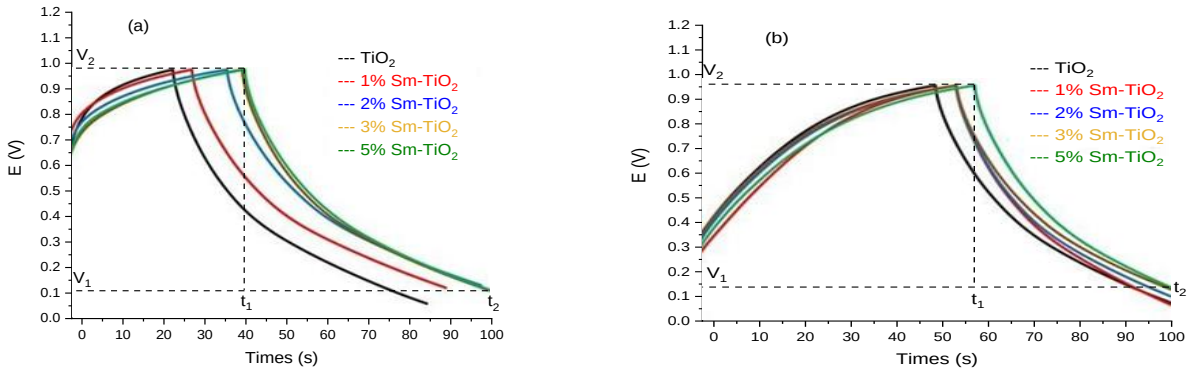

Figure 12. Chronopotentiometric curves of pure and Sm-TiO_2 (a) dark, and (b) illumination with 2mM current density

The charge-discharge demeanor and the ability of the synthesized Sm-TiO_2 catalyst for capturing the charges were investigated via double step chronopotentiometry (CP). As shown in Fig. 12a,b the measurements were conducted by administering 0.05A/m^2 in both directions of oxidation and reduction under dark and illumination conditions. The charging curve exhibited a gradual increase in potential until it reached a plateau, whereas the discharging curve showed a sharp drop followed by a gradual decrease in potential. When compared to other electrodes, 5% Sm-TiO_2 decayed at a slower rate under lights. The lack of electrochemical double layer qualities was noticed instead of pseudo capacitive attitude for curves of charge-discharge of varied electrodes modified with anatase TiO_2 and Sm-TiO_2 catalyst, implying electrochemical reversibility and outstanding capacitive properties. The specific capacitance of synthesized photocatalyst was calculated by utilizing the following equation [34]: (Eq.3)

$$C_s = \frac{I \times \Delta t}{m \times \Delta V} \quad 3$$

Where: Cs is specific capacitance in (F/g), I: current of discharge in (mA), t: time of discharge in (s), V: drop of potential during discharge in (V) and m: is the mass of active material loaded on the electrode in (mg). The results show that the specific capacitance of electrodes under illumination condition are 110.5, 122.6, 125.1, 126.5 and 129.5 (F/g) corresponding to TiO_2, 1%, 2%, 3% and 5% of Sm-TiO_2 respectively, which means as the Sm^{3+} loading was raised, the ability to capture and maintain charge improved.

4. CONCLUSION

In this study, the anatase phase and Sm-TiO_2 were successively synthesized by photolysis method. The samples were characterized by XRD, FESEM-EDX, XPS, Raman and UV-Vis. The Sm:TiO_2 powder consist of spherical nanoparticles with 5.197 nm particles size. The band gap was estimated to be 2.86eV for %5 Sm:TiO_2 and decreased with increasing Sm^{3+} concentration. The efficiency of particles was examined by degrading RhB dye under sunlight with maximum degradation efficiency of 89%. The electrochemical results show that the catalyst behaves as a pseudocapacitor when the Sm^{3+} ratio rises, as does the conductivity.

DATA AVAILABILITY
All data generated or analyzed during this study are included in this published article

CONFLICT OF INTEREST
We wish to confirm that there are no known conflicts of interest associated with this publication and there has been no significant financial support for this work that could have influenced its outcome.

References

1. A. Alhujaily, H. Yu and X. Zhang, *Appl. Water. Sci.,* 10 (2020) 183.
2. M.F. Abou Taleb, F.I. Abou El Fadl and H.A. Albalwi, *J. Inorg. Organomet. Polym.,* 31 (2021) 1395.
3. H. Seifi and S. Masoum, *J. Iran. Chem. Soc.*, 17 (2020) 2969.
4. A.S. Assémian, K.E. Kouassi and P. Drogui, *Water Air Soil Pollut.,* 229 (2018) 184.
5. M. Joshi, R. Bansal and R. Purwar, *Indian J. Fibre Text. Res.,* 29 (2004) 239
6. A.K Verma, R.R Dash and P. Bhunia, *J. Environ. Manag*., 93 (2012) 154.
6. P.K. Singa, M.H. Isa and J.W. Lim, *Int. J. Environ. Sci. Technol*., 18 (2020) 3515.
7. B.G.H. Briton, L. Duclaux and Y. Richardson, *Appl Water Sci.,* 9 (2019) 166.
8. P. Kokkinos, D. Venieri and D. Mantzavinos, *Food Environ Virol*., 13 (2021) 283.
9. S. Li, L. Chen and Z. Ma, *Trans. Tianjin. Univ.,* 27 (2021) 295.
10. S. Malato, P. Fernández-Ibáñez, M.I. Maldonado, J. Blanco and W. Gernjak, *Catal. Today,* 147 (2009) 1.
11. P.H. Allé, G.D. Fanou and D. Robert, *Appl Water Sci.,* 10 (2020) 207.
12. Y. Xie and C. Yuan, *Appl. Surf. Sci.,* 221 (2004) 17.
13. F.B. Li, X.Z. Li, M.F. Hou, K.W. Cheah and W.C.H. Choy, *Appl. Catal., A* 285 (2005) 181.
14. D.P. Macwan, P.N. Dave and S. Chaturvedi, *J. Mater. Sci.,* 46 (2011) 3669.
15. K.H. Lee and W. Song, *ACS Appl. Mater. Interfaces,* 3 (2011) 3697.

16. N. Nithya, E.R. Kumar and G. Magesh, *J. Mater. Sci.: Mater. Electron.,* 32 (2021) 16854.
17. Z.H. Mahmoud and R.F. Khudeer, *Int. J. Chemtech Res.,* 12 (2019) 64.
18. Li. Wei, Y. Yang, X. Xia, R. Fan, T. Su, Y. Shi, J. Yu, L. Li and Y. Jiang, *RSC Adv.,* 5 (2015) 70512.
19. G.V. Khade, M.B. Suwarnkar and N.L. Gavade, *J. Mater. Sci.: Mater. Electron.,* 27 (2016) 6425.
20. L. Gomathi, B. Narasimha and S. Girish, *Mater. Sci. Eng., B* 166 (2010) 1.
21. C.Y. Xu, P.X. Zhang and L. Yan, *J. Raman Spectrosc.,* 32 (2001) 862
22. T. Ohsaka, *J. Phys. Soc. Jpn.*, 48 (1980) 1661.
23. R.T. Liu, Y. Qiao, Y. Bie and Y. Song, *Bull. Mater. Sci.,* 42 (2019) 239.
24. J. Szlachetko, K. Michalow-mauke and M. Nachtegaal, *J. Chem. Sci.,* 126 (2014) 511.
25. A. Hameed, M. Aslam, I.M.I. Ismail, S. Chandrasekaran, M.W. Kadi and M.A. Gondal, *Appl. Catal., B* 160–161 (2019) 227.
26. P. Pichat, Photocatalysis and water purification: from fundamentals to recent applications (1st ed.), Wiley-VCH, (2013) Germany.
27. M.A. Henderson, *Surf. Sci. Rep.,* 66 (2011) 185.
28. H. Mashiko, T. Oshima and A. Ohtomo, *Appl. Phys. Lett.,* 99 (2011) 241904.
29. Y.T. Liu, Q.B. Yuan, D.H. Duan, Z.L. Zhang, X.G. Hao, G.Q. Wei and S.B. Liu, *J. Power Sources,* 243 (2013) 622.
30. M. Hameed, I.M.I. Ismail, A. Aslam and M.A. Gondal, *Appl. Catal., A* 470 (2014) 327.
31. M.T. Qamar, M. Aslam, Z.A. Rehan, M.T. Soomro, I. Ahmad, M. Ishaq, I.M.I. Ismail, P. Fornasiero and A. Hameed, *Chem. Eng. J.,* 330 (2017) 322.
32. M. Aslam, M.T. Qamar, M.T. Soomro, I.M.I. Ismail, N. Salah, T. Almeelbi, M.A. Gondal and A. Hameed, *Appl. Catal., B* 180 (2016) 391.
33. L. Yu and G. Chen, *Electrochem. Energy Rev.*, 3 (2020) 271.